Tellus (1996), 48A, 138–157
Printed in Belgium – all rights reserved

TELLUS
ISSN 0280–6495

An investigation of the general circulation of the Arctic Ocean using an isopycnal model

By DAVID M. HOLLAND[1]* and LAWRENCE A. MYSAK, *Department of Atmospheric and Oceanic Sciences and Centre for Climate and Global Change Research, 805 Sherbrooke Street West, McGill University, Montréal, Québec H3A 2K6, Canada* and JOSEF M. OBERHUBER, *German Climate Computer Centre, Bundesstrasse 55, 20146 Hamburg, Germany*

(Manuscript received 17 November 1994; in final form 2 May 1995)

ABSTRACT

A numerical simulation of the general circulation of the Arctic Ocean is presented using Oberhuber's (1993a) coupled sea ice, mixed layer, isopycnal general circulation model (OPYC). The model's novel feature is that the ocean component uses density surfaces as the vertical coordinate. The model domain includes the Arctic Ocean, the Greenland-Iceland-Norwegian (GIN) Sea, and the North Atlantic Ocean. The horizontal resolution is 1.0° in a spherical coordinate system that is rotated with respect to geographical coordinates. The vertical is resolved into eleven isopycnal layers of which the uppermost layer is a turbulent mixed layer. The sea ice is modelled using the dynamic-thermodynamic model of Oberhuber which incorporates the Hibler viscous-plastic rheology. A restriction of the coupled model used here is the artificial placement of solid walls across the Bering Strait and at the equator in the Atlantic Ocean. Monthly climatological atmospheric forcing is used to spin the model into a cyclo-stationary equilibrium. Model results are presented and discussed with respect to observational and previous modelling studies. The simulated water mass properties and circulation are in reasonable agreement with observations. Based on the simulation results, new circulation patterns are suggested for the deep flow within the Arctic Ocean. In particular, it is proposed that for the Atlantic layer and deeper waters there exists a multi-gyre circulation pattern consisting of cyclonic gyres that essentially follow contours of bottom topography.

1. Introduction

This paper investigates the general circulation of the Arctic Ocean using the coupled sea ice, mixed layer, isopycnal ocean general circulation model (OPYC) developed by Oberhuber (1993a). Recent research in physical oceanography and climate in the Arctic has focused on understanding the nature and variability of the sea-ice cover in the ocean and also on determining the general circulation of the subsurface waters (Mysak and Power, 1992; Aagaard, 1989). Although simulation results of the sea-ice and mixed layer are briefly presented here, this paper focuses on the simulation of the circulation and water-mass properties below the mixed layer. The reader is referred to Holland et al. (1995) for a detailed discussion of the mixed-layer circulation and its sensitivity to model parameters and parameterizations. Some of the observational and modelling studies that have been carried out are briefly reviewed below.

1.1. *Observed features*

A review of the large-scale physical oceanography of the Arctic Ocean has been presented by Carmack (1990). He discusses in detail the bathymetry, hydrology, ice cover, water masses, and

* Corresponding author.
[1] Now at Lamont-Doherty Earth Observatory of Columbia University, PO Box 1000, Route 9W, Palisades, New York, 10964-8000, USA.

current systems. The most salient features are highlighted below.

The Arctic Basin (hereafter simply referred to as the basin) is deep, with an average depth of about 4000 m (Fig. 1a). It consists of two basins, the Canadian and the Eurasian Basins, which are separated by the Lomonosov Ridge. The ridge is at a depth of 1500 m below the surface and extends across the basin from Siberia to Greenland. In the data set used to create the basin bathymetry, there is a slight break in the ridge near the pole (Fig. 1a). The Arctic communicates with the Atlantic Ocean via the relatively wide (460 km) and deep (2500 m) Fram Strait; by contrast, communication with the Pacific Ocean occurs through the much narrower (65 km) and shallower (45 m) Bering Strait. Exchanges also occur with the Canadian Arctic Archipelago and the Barents Sea.

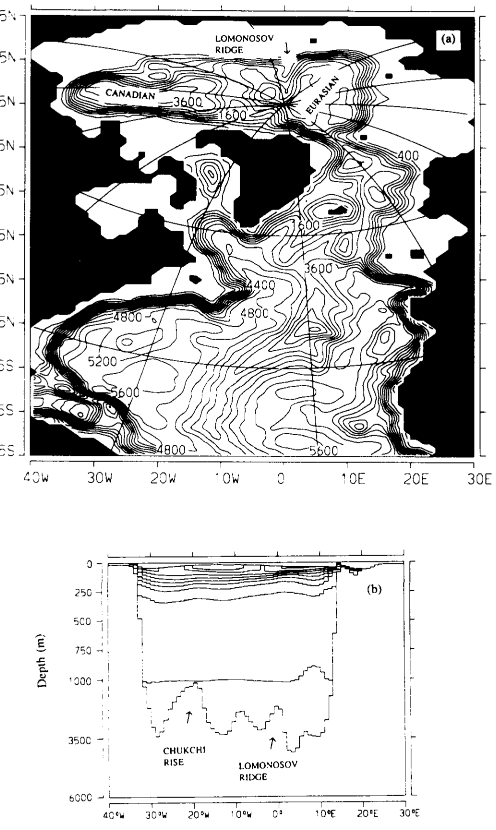

Fig. 1. The model's horizontal and vertical space. (a) Bathymetry (m) of the entire model domain. The black areas represent land. The coordinates labelled along the axes are in rotated model coordinates. The thin lines superimposed on the figure are the geographical latitudes and longitudes. Contour interval is 400 m. (b) An example of the model's vertical Lagrangian coordinate system. See text for details.

The waters entering via Bering Strait are much fresher (30 psu) than those entering through Fram Strait (35 psu). Since the typical surface waters of the Arctic Ocean have a salinity of 32 psu, the Bering Strait flow contributes substantially to the freshwater influx to the basin (2000 km^3/yr). An even greater influx of freshwater is produced by the numerous rivers located along the periphery of the basin (3500 km^3/yr) (Aagaard and Carmack, 1989).

The net transport of sea water into the basin via Bering Strait is estimated to be 0.8 Sv (Aagaard and Carmack, 1989). This is considerably smaller than the Fram Strait flows which are composed of an influx of about 7 Sv of warm, saline water (the West Spitsbergen Current) and an outflow of about 7 Sv of relatively cool, fresh water (the East Greenland Current). The water column is considered to be composed of three main layers: a cold-fresh surface layer (0 to 200 m depth) which is influenced by the sea-ice formation and river runoff, a warm, saline intermediate layer (200 m to 900 m) due to an influx from the Atlantic via the West Spitsbergen Current, and a deep (900 m to the bottom) cold, saline layer formed by convection. The water column in the Canadian basin is much more stably stratified than in the Eurasian basin. The salinity distribution in the surface layer clearly reflects the influx of saline Atlantic water through Fram Strait. Similarly, the temperature distribution in the core of the Atlantic layer shows a tongue of warm water which indicates the penetration of warm Atlantic water through Fram Strait.

Inside the basin, the surface flow is believed to consist of the anticyclonic Beaufort gyre in the Canadian basin and the transpolar drift stream, directed towards Fram Strait, in the Eurasian basin. The flow of sea ice follows this pattern as well. According to Carmack (1990), the Atlantic layer flow consists of a cyclonic circulation in each of the Canadian and Eurasian basins. The deeper flow is generally believed to be similar to that of the Atlantic layer. However, recent results inferred from tracer measurements suggest that the subsurface circulation may in fact consist of several cyclonic gyres (Rudels et al., 1993; E. P. Jones personal communication, 1992).

1.2. Previous modelling results

Galt (1973) carried out the first large-scale modelling study of the Arctic Ocean. He solved a barotropic vorticity equation forced by the curl of the wind stress. The resulting flow consisted of an anticyclonic Beaufort gyre and a transpolar drift stream directed towards Fram Strait (Fig. 14). This was a wind-driven flow which ignored the thermohaline circulation and the exchange of water masses through various straits.

Semtner (1976) used a baroclinic ice-free model which simulated the anticyclonic surface flow of the Beaufort gyre (Fig. 7). He obtained a stable stratification characterized by a halocline. The Eurasian basin received both an intermediate layer of warm Atlantic water and bottom water from the west Spitsbergen current, and it exported surface water of low salinity into an intense east Greenland current. However, the sense of circulation in the Atlantic layer (Fig. 10) in the central Arctic was opposite to that inferred from water-mass properties.

The first coupled sea ice, ocean model was presented by Hibler and Bryan (1987). Although they emphasized the sea-ice simulation, some results were presented for the ocean surface circulation. The modelled flow showed an anticyclonic Beaufort gyre and a transpolar drift stream (Fig. 11). Results for the deeper circulation were not presented since the model was diagnostically constrained below the surface layer.

Semtner (1987) presented a coupled sea, ice ocean model in which the diagnostic constraint of Hibler and Bryan was removed and a simpler ice rheology was employed. The ocean circulation in the Canadian basin was anticyclonic at all depths, but changed to cyclonic in the Eurasian basin below 200 m. He was able to simulate the inflow of warm Atlantic water into the Arctic basin (Fig. 12); however, the spatial distribution of temperature across the basin did not mimic the observed pattern.

Further modelling efforts to study the Arctic Ocean climatology have been carried out using coupled sea ice, ocean models, e.g., Ranelli and Hibler (1991), Ries and Hibler (1991), Warn-Varnas et al. (1991); however, the focus has been on the sea-ice simulation and not on the ocean circulation and water-mass properties. To date, almost all modelling studies have been based on a variant of the Bryan–Cox ocean model (Cox, 1984). Part of the motivation for the present work is the availability of a new ocean general circulation model (OPYC) that has been developed by Oberhuber (1993a). This new model differs from the Bryan–Cox model in that it uses isopycnal surfaces as the vertical coordinate. The vertical coordinate is thus Lagrangian rather than Eulerian. The flow in the horizontal plane is then naturally directed along isopycnal surfaces. This new model is applied to the Arctic basin with the goal of obtaining an improved simulation of the water mass and circulation properties, most of which have not been correctly simulated in previous studies.

The remainder of this paper is organized as follows. Section 2 briefly describes the coupled sea ice, mixed layer, isopycnal ocean model. The simulation results for the sea-ice, mixed-layer, and deep-ocean isopycnal-layer models are presented in Section 3. Section 4 highlights the key results of the paper.

2. The model

The application of the Oberhuber (1993a) model in the present work is distinct from that of Oberhuber (1993b). In that latter paper, Oberhuber discussed principally the circulation of the North Atlantic and not that of the Arctic, which is the focus of this paper. It is worth noting that the OPYC model has recently been successfully applied to a study of the GIN Sea (Aukrust and Oberhuber, 1994), thus lending some confidence to its application to the Arctic.

The OPYC model consists of three coupled submodels. The sea-ice is represented by a dynamic-thermodynamic model with viscous-plastic rheology (Oberhuber et al., 1993), the mixed layer by a turbulent kinetic energy model (similar to models due to Niiler and Kraus (1977), and Garwood et al. (1985)), but with Ekman-depth dependent dissipation terms), and the deep ocean by an isopycnal-layer model. The models interact via the exchange of momentum, mass, heat and salt. Forcing occurs via the specification of monthly climatological atmospheric fields, and realistic topography is employed. The equations describing each model are fully described by Oberhuber (1993a). They are briefly presented here to highlight the physical processes that are represented. This section ends by describing the physical layout of the model.

2.1. Sea ice

For the momentum balance, the ice is considered to move in a two-dimensional spherical plane with forcing fields operating on the ice via simple planetary boundary layers. The nonlinear inertial terms are neglected. The equation is

$$\frac{\partial \boldsymbol{u}h}{\partial t} = \nabla \cdot A^m \nabla \boldsymbol{u}h - \boldsymbol{f} \times \boldsymbol{u}h - gh\, \nabla \Gamma + \frac{\boldsymbol{\tau}_a}{\rho_i} + \frac{\boldsymbol{\tau}_o}{\rho_i} + \frac{\boldsymbol{I}}{\rho_i}, \tag{1}$$

where $\boldsymbol{u} = (u, v)$ is the horizontal velocity vector, h the ice thickness, A^m the horizontal diffusion coefficient for momentum, f the Coriolis vector, g the acceleration due to gravity, Γ the sea surface dynamic height, ρ_i the ice density, $\boldsymbol{\tau}_a$ the ice surface wind stress, $\boldsymbol{\tau}_o$ the ice bottom current stress, and $\boldsymbol{I}$ the internal ice stress which is based on a viscous-plastic ice rheology (Hibler, 1979).

The snow-cover thickness s and the ice-cover thickness h are modelled as continuous non-negative variables. The presence of leads in the ice is modelled using a variable called the ice compactness q and is defined as the fraction of a grid cell area covered by ice; the rest of the cell is covered by open water. The spatial and temporal variations in snow and ice thickness and ice compactness are modelled by the continuity equations

$$\frac{\partial s}{\partial t} = -\nabla \cdot (\boldsymbol{u}s) + \nabla \cdot A^s\, \nabla s + F_s - F_a, \tag{2}$$

$$\frac{\partial h}{\partial t} = -\nabla \cdot (\boldsymbol{u}h) + \nabla \cdot A^s\, \nabla h + F_h + F_a, \tag{3}$$

$$\frac{\partial q}{\partial t} = -\nabla \cdot (\boldsymbol{u}q) + \nabla \cdot A^s\, \nabla q + F_q, \tag{4}$$

where F_s, F_a, F_h, and F_q are thermodynamic forcing or source terms (Oberhuber et al., 1993; Holland, 1993, for a discussion of these terms). The numerical diffusion terms for these scalar equations have the same coefficient A^s.

2.2. Mixed layer

The sea-ice and deep-ocean models are coupled through an ocean mixed-layer model. The mixed layer has vertically uniform velocity, density, temperature and salinity. This uniformity is produced by both wind-stirring and surface buoyancy fluxes. The mixed-layer depth is controlled by both local mixing and the horizontal convergence of mass and heat. The mixed layer is in fact the uppermost layer of the deep-ocean model and it always has a nonzero thickness and a temporally and spatially varying potential density. This is in contrast to all deeper layers which may have a zero thickness and always have a prescribed potential density.

The mixed layer differs from the deeper layers in that it is directly forced by a surface buoyancy flux due to heat and freshwater fluxes. As a result, the mixed layer depth, h_1, changes through the processes of entrainment and detrainment. The equation for the entrainment rate w is

$$wg'h_1 - w\,\mathrm{Ri}_c(\Delta u^2 + \Delta v^2) = au_*^3 + bB, \tag{5}$$

where g' is the reduced gravity, Ri_c the critical Richardson number, Δu^2 and Δv^2 the square of the difference in velocity component between the mixed layer and the layer below it, a and b weighting coefficients, u_* the friction velocity, and B the surface buoyancy flux. The first term on the left hand side of eq. (5) describes the production of mean potential energy due to the vertical displacement of isopycnals; the second term describes the production of mean kinetic energy due to vertical velocity shear. On the right-hand side, the first term stands for the production of turbulent kinetic energy due to wind stirring; the second term is the buoyancy flux which is induced by heat and fresh water fluxes.

In ice-covered regions, there are modifications to the mixed-layer entrainment/detrainment processes (i.e., eq. (5)) which are discussed in Oberhuber (1993a).

2.3. Deep ocean

The representation of the oceanic flow along isopycnal layers is motivated by the assumed adiabatic nature of the subsurface ocean. In the Arctic, isopycnal coordinates are particularly appropriate because of the high stability of the water column. The use of isopycnal coordinates allows flow to occur naturally along isopycnal surfaces. At the same time, the model poses certain challenges in trying to represent such phenomenon as the intersection of isopycnal surfaces either with the sea surface or with the bathymetry, cross-isopycnal mixing and convection.

As mentioned earlier, the model discretizes the water column (below the mixed layer) into layers of prescribed potential density. Both the depth of a layer beneath the surface and its thickness vary temporally and spatially due to mass flux divergence, entrainment, and cross-isopycnal mixing. A layer is permitted to migrate vertically up or down, increase or decrease its thickness, and intersect with the mixed layer or bathymetry. This freedom of movement allows the model to optimally represent a highly stratified water column by having many thin isopycnal layers near the pycnocline. At the same time, the model can represent a well mixed water column by a few relatively thick layers. The benefit of isopycnal coordinates is that as the water column changes its stratification either spatially or temporally, the coordinate system adjusts to adequately represent it.

Within each layer (of depth h say) the mass flux, the mass content, the heat content, and the salt content are prognostically computed. The basic equations are formulated in flux form and represent conservation equations for the vertically averaged mass flux ($\boldsymbol{u}\rho h$), mass content (ρh), heat content ($\theta\rho h$), and salt content ($S\rho h$):

$$\frac{\partial(\boldsymbol{u}\rho h)}{\partial t} = -\nabla(\boldsymbol{u}(\boldsymbol{u}\rho h)) - h\,\nabla p - \boldsymbol{f}\times(\boldsymbol{u}\rho h) + \nabla\cdot A^m\,\nabla(\boldsymbol{u}\rho h) + \Omega[\rho\boldsymbol{u}] + \boldsymbol{\tau}, \tag{6}$$

$$\frac{\partial(\rho h)}{\partial t} = -\nabla\cdot(\boldsymbol{u}\rho h) + \Omega[\rho] + R^{P-E+R}, \tag{7}$$

$$\frac{\partial(\theta\rho h)}{\partial t} = -\nabla\cdot(\boldsymbol{u}(\theta\rho h)) + \nabla\cdot A^s\,\nabla(\theta\rho h) + \Omega[\theta\rho] + \frac{Q}{c_p}, \tag{8}$$

$$\frac{\partial(S\rho h)}{\partial t} = -\nabla\cdot(\boldsymbol{u}(S\rho h)) + \nabla\cdot A^s\,\nabla(S\rho h) + \Omega[S\rho] + R^I, \tag{9}$$

where $\boldsymbol{u} = (u, v)$ is the horizontal layer velocity, h the thickness, θ the potential temperature, S the salinity, ρ the potential density, p the in situ pressure, $\boldsymbol{f}$ the Coriolis vector, A^m the diffusion coefficient for momentum, A^s the diffusion coefficient for heat and salt, $\Omega[\gamma]$ the cross-isopycnal transfer of a quantity γ, $\boldsymbol{\tau}$ the stress between neighbouring layers, Q the heat flux into a layer, c_p the specific heat capacity, R^{P-E+R} the fresh water flux due to precipitation minus evaporation plus river runoff, and R^I the fresh water flux due to the sea ice, ocean coupling.

The omega terms in eqs. (6)–(9) are unique to the isopycnal formulation of the present model. These terms represents the cross-isopycnal transfer of quantities due to convection. They also represent the cross-isopycnal transfer of those quantities required for the model to maintain its vertical coordinate system. As an example, if water in a given layer converges at a grid point, then it may be that this water mass is too light (heavy) to remain in its present isopycnal layer. This situation may arise either due to the real physical process of cabbeling or due to numerical roundoff errors. This water is then pumped into the layer above (below) with an appropriate isopycnal density. This is fundamentally how an isopycnal model maintains its coordinate system.

2.4. *Model layout*

The domain chosen for this study includes the Arctic Ocean, the Greenland-Iceland-Norwegian (GIN) Sea, and the North Atlantic. The motivation for including the North Atlantic is the need to simulate the influx of warm, saline water into the GIN Sea from the North Atlantic as well as the outflow of cold, fresh water from the Arctic. The model places a solid wall across the southernmost boundary of the domain, which is located near the equator at 10° N in the Atlantic Ocean. A realistic simulation of the interhemispheric thermohaline circulation is thus not possible as cross-equatorial flow is a priori blocked. However, a single hemisphere thermohaline circulation is simulated in the model. Possibly of greater consequence to the Arctic circulation is the artificial boundary placed across the Bering Strait; thus the model does not allow for the inflow of warm, fresh Pacific water via Bering Strait. The magnitude of the missing flux is of order 0.8 Sv. The Canadian Arctic archipelago is open and does permit the flow of cold, fresh Arctic Surface water into Baffin Bay.

The model's bathymetry is obtained by interpolating a high resolution (5 min) topographic data set onto the model's grid. The main bathymetric features of the Arctic basin are identified in Fig. 1a, i.e., the Canadian and Eurasian Basins, and the Lomonosov Ridge. Since the focus of this paper is the Arctic, simulation results will focus on the Arctic portion of the total model domain.

A problem with numerical models written in spherical coordinates for the Arctic Ocean is the convergence of the east-west grid spacing near the North Pole. The non-uniformly varying grid spacing near the Pole implies artificially reduced signal-speed (e.g., for transports) when an implicit numerical technique, as is done here, is employed. This is overcome by rotating the model coordinates by Eulerian angles such that the model coordinates converge to a point in Siberia, which is outside the defined model domain. All figures presented in this paper indicate the rotated latitude and rotated longitude coordinates along their axes.

The model resolves the water column using eleven vertical layers of prescribed potential density. An example of the vertical coordinate is shown in Fig. 1b as a vertical transect running across the domain from west to east at a rotated latitude of 61°N (see Fig. 1a for orientation). The upper most layer is the first isopycnal layer with a reference potential density of 1024.07 kg/m^3. The water column beneath this first layer is resolved using up to ten isopycnal layers with successively deeper layers having density values of 1024.48, 1024.88, 1025.28, 1025.69, 1026.09, 1026.49, 1026.90, 1027.30, 1027.70, and 1028.11 kg/m^3.

The initially prescribed density and thickness of each layer are obtained via interpolation of the temperature and salinity data of Levitus (1982). Densities are computed using the fully nonlinear UNESCO equation of state. As the model integrates in time, the layer thicknesses vary in time and space; however, the densities do not. The first layer, which is the mixed layer, is allowed to change its potential density in response to entrainment and surface buoyancy fluxes. At any instant all layers may be present, or one or more may be absent as the result of mass flux divergence or of detrainment from that layer into neighbouring layers. At a later time, a layer may reappear as the result of mass flux convergence or entrainment into that layer. In this manner the layers both migrate in the vertical coordinate direction as well as change their thickness. Where the water column is highly stratified, more layers are required to resolve the vertical structure than when the water column is well mixed. The vertical coordinate scheme adopted automatically satisfies this demand.

The model uses spherical coordinates in the horizontal with a resolution of 1.0° in latitude and longitude. Since the model coordinates are rotated by Eulerian angles with respect to geographical coordinates, the spatial resolution is about 80 km in the Arctic. Thus, the grid spacing resolves the flow through Fram and Denmark Straits; however, the spacing is substantially larger than the internal Rossby radius ($\sim$10 km). The horizontal resolution can be inferred from Fig. 2 which shows the wind stress forcing.

The model is forced using monthly climatological fields of wind stress, radiation, air temperature, humidity, rainfall and cloud cover. These fields are described by Oberhuber (1988), Wright (1988), Trenberth et al. (1989), and Legates and Willmott (1990). The model derives the forcing at a particular time step by linearly interpolating between climatological fields of neighbouring months.

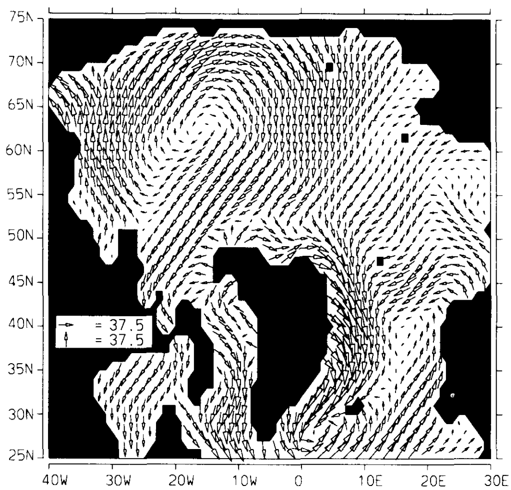

Fig. 2. Observed wind stress (mN/m^2) on 1 April. A large-scale anticyclonic gyre is evident over the Arctic basin. Also, there is a strong flow directed across the Eurasian basin towards Fram Strait.

The model is spun up using a multi-grid approach in an effort to minimize computational cost. The model is integrated on a 2.0° latitude/longitude grid for a period of 50 years using the Levitus (1982) data as initial conditions. The model resolution is then increased to a 1.0° latitude/longitude grid for a final integration of an additional 20 years. This is an adequate time for the sea-ice and mixed-layer models to reach an equilibrium; however, the deep-ocean circulation almost certainly is not in complete equilibrium after such a short period, that is, there may still be a residual drift in the properties of the deeper waters. One simulated year requires two hours of CPU time on a Cray-YMP; consequently, integrations for thousands of years are not feasible.

The salinity structure of the surface waters is the result of the processes of advection, diffusion, vertical mixing, ice growth/melt, precipitation (generally snow), evaporation, and river runoff. These terms can be identified on the right-hand-side of eqs. (7) and (9). For the Arctic, the ice growth/melt contribution is prognostically computed from the sea-ice model; however, the river runoff is diagnostically specified using the nine Arctic rivers as described in Aagaard and Carmack (1989, their Fig. 3). The river inflow is specified in such a way that the vast majority of the river water enters the Arctic during the summer. The precipitation is handled in such a way that snow (diagnostically) falls on the ice, is then transported by the ice, and finally melts when the ice melts or the surface energy budget forces it to melt (summer). The current state of ocean modelling is such that it is necessary to add a relaxation term (towards the observed salinity) in order to achieve an accurate simulation. The relaxation to the observed monthly salinity field corrects for errors in the model's treatment of advection, diffusion, vertical mixing, ice growth/melt, precipitation, evaporation and river runoff. The time constant with which the actual salinity relaxes to the observed salinity is one month.

The model, as adapted for this study, ignores the inflow of mass and momentum from the Bering Strait. However, in terms of salt transport, the effect of the Bering Strait is in essence modelled because we relax the surface salinity to the observed salinity. This results in a realistic sea surface salinity field near Bering Strait.

The temperature is not directly relaxed to the observed ocean values; instead, sea surface temperature is essentially relaxed to an apparent surface temperature that is obtained from a complete surface energy balance that includes longwave, shortwave, sensible and latent heat terms (see Oberhuber, 1993a, for details).

Prior to analyzing the model's simulation of the general circulation, it must be established that the model has reached a cyclo-stationary equilibrium. Time-depth diagrams of temperature and salinity for the 20 years of integration performed on the 1.0° grid are constructed for locations in both the central Canadian and Eurasian Basins. As mentioned above, the model is first integrated on a 2.0° grid, starting from Levitus data, for 50 years. The time-depth diagrams (not shown) for temperature and salinity indicate that the model is not satisfied with the Levitus data and evolves substantially away from these during the initial 50 year integration period. At the end of the 50 year period, the deeper (below 1000 m) temperature and salinity fields are still evolving. At 50 years, the model grid is then switched to a 1.0° grid and integrated, starting from the model state at the end of the 50 years on the 2.0° grid, for an additional 20 years (see Fig. 3). During this final 20 year period, the deeper temperature and salinity do tend towards equilibrium values, although there is a small drift at depth.

It is apparent (Fig. 3a, b) that the temperature of the Atlantic Layer (i.e., between 300 and 900 m depth) is too warm (by about 1.0°C) in both the Canadian and Eurasian Basins. Apparently, the model does not at present have the correct process that in allows the Atlantic Layer to lose heat sufficient heat. The most likely improvement to the model will come in the treatment of convection processes on the continental shelf that would allow the detrainment of cold, saline shelf water out of the mixed layer and down into the Atlantic layer. Although the temperature of the Atlantic layer water is too high, it is encouraging to see the Atlantic layer water occurring at approximately the correct depth interval (i.e., 300 to 900 m) as well as the fact that it is simulated to be thinner in the Canadian basin (Fig. 3a) than in the Eurasian basin (Fig. 3b). A previous model run had used nine isopycnal layers and simulated the Atlantic layer at a depth too far down in the water column. The depth-time diagram for the Canadian basin (Fig. 3a) shows that equilibrium is reached after

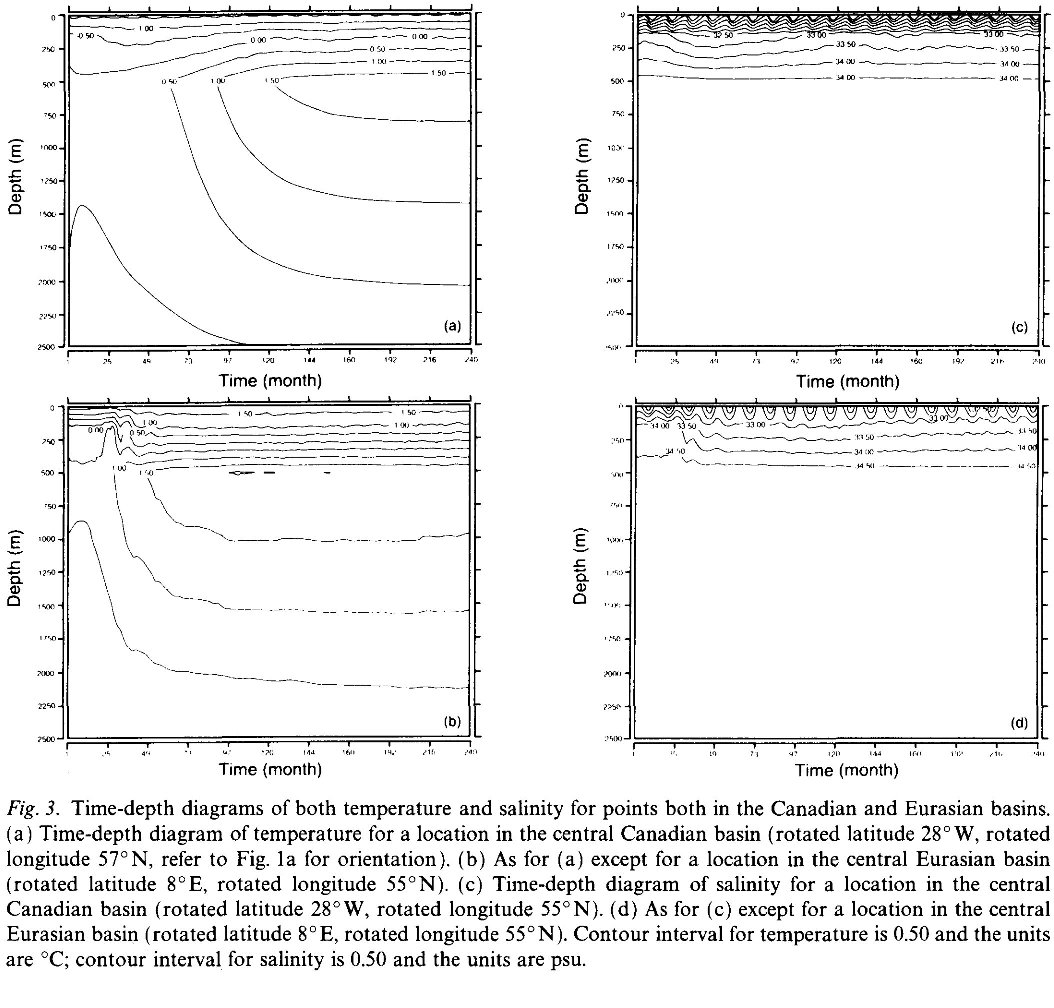

Fig. 3. Time-depth diagrams of both temperature and salinity for points both in the Canadian and Eurasian basins. (a) Time-depth diagram of temperature for a location in the central Canadian basin (rotated latitude 28° W, rotated longitude 57° N, refer to Fig. 1a for orientation). (b) As for (a) except for a location in the central Eurasian basin (rotated latitude 8° E, rotated longitude 55° N). (c) Time-depth diagram of salinity for a location in the central Canadian basin (rotated latitude 28° W, rotated longitude 55° N). (d) As for (c) except for a location in the central Eurasian basin (rotated latitude 8° E, rotated longitude 55° N). Contour interval for temperature is 0.50 and the units are °C; contour interval for salinity is 0.50 and the units are psu.

about 15 years of the 1.0° run; by contrast the Eurasian basin (Fig. 3b) reaches equilibrium after about 10 years. This is to be expected as the source for the Atlantic layer water (i.e., Fram Strait) is geographically closer to the Eurasian basin.

The time-depth diagrams for salinity (Fig. 3c, d) show that equilibrium in salinity is also established after 20 years of the 1.0° run. The variations in salinity are confined to the upper 500 m of the water column. The pycnocline in the Canadian basin (Fig. 3c) is much stronger than in the Eurasian basin (Fig. 3d) as is indeed observed in reality (Carmack, 1990). In the simulation, the surface salinity is relaxed to the observed salinity of Levitus (1982), thus it is not surprising that the stratification is stronger in the Canadian basin compared to the Eurasian.

3. Simulation results

The purpose of this section is to give a snapshot of the model's simulation of the sea-ice and ocean circulation of the Arctic Ocean. Results are generally only shown for one particular day, i.e., 1 April, this being representative of conditions at the end of winter. The sea-ice and the mixed-layer do undergo considerable variation over an annual cycle, and these seasonal variations are discussed in related studies by Holland et al. (1993, 1995) and Oberhuber et al. (1993). Here we focus on the deeper circulation, which is quite steady.

3.1. Sea ice

The sea-ice velocity field (Fig. 4a) and thickness field (Fig. 4b) represent reasonable simulations as compared to observations. The sea-ice module of OPYC has recently been modified. In particular, improvements have been made in the treatment of the important sea-ice rheology terms. Essentially, these terms are now treated implicitly in a single step; previously a two-step predictor-corrector technique was employed. The result is that the new formulation can use more realistic values for certain ice rheology parameters than was possible earlier; the strength parameter used is $P^* = 30{,}000\ \mathrm{N/m^2}$, while the minimum strain rate used is $\varepsilon_o = 10^{-8}\ \mathrm{s^{-1}}$. This modified code is being used in the simulations presented in this paper.

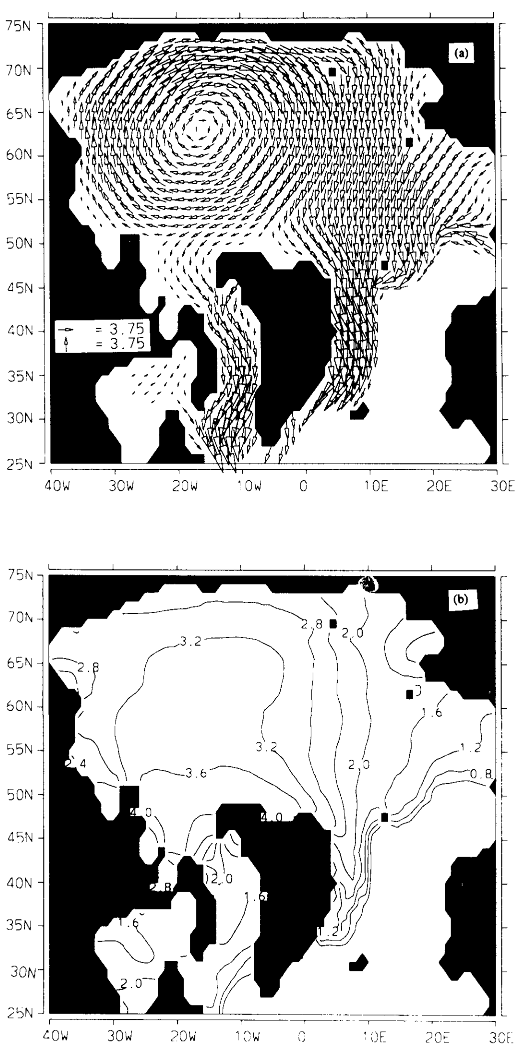

Fig. 4. (a) Sea-ice velocity (cm/s) for 1 April. (b) Sea-ice thickness (m) for 1 April. A surrogate for the ice-edge position is given by the 0.4 m thickness contour. Contour interval is 0.4 m.

The velocity field of Fig. 4a indicates a large anticyclonic gyre which spans the entire Arctic basin; this is in agreement with observations by Colony et al. (1991). This sea-ice circulation pattern mimics the pattern of the wind stress (Fig. 2) used to force the model. Thus, the winds are evidently dominating the sea-ice motion. The ice exits the basin at a relatively high-speed (i.e., 10 cm/s) flow southward through Fram Strait. The thickness field of Fig. 4b indicates that the thickest ice occurs along the northern coast of Greenland and along the Canadian Arctic archipelago, which is consistent with what is observed (Bourke and Garrett, 1987).

3.2. Mixed layer

The sea-surface velocity pattern is representative of the subtropical and subpolar gyres in the North Atlantic (not shown). The dominant northward currents are the Gulf Stream and its extension as the North Atlantic current, which ultimately becomes the Norwegian Sea current. The dominant southward currents are the east Greenland current and the Labrador current. Fig. 5 shows that there is a flow from the Western Arctic, into the Canadian Arctic archipelago, and on into Baffin Bay. In the Arctic basin, the dominant flow feature is a large anticylonic gyre whose northern branch extends from the Bering Strait along the continental shelf break of the Chukchi and East Siberian Seas. Part of the flow turns right and flows parallel to the Lomonosov Ridge as the Transpolar Drift Stream, and finally exits the Arctic basin through Fram Strait. Another part of this flow continues along the continental shelf break in the East Siberian Sea and into the Laptev Sea where it then follows the continental shelf break of the Barents Sea until it finally makes its way towards Fram Strait.

In the lower left-hand part of Fig. 5, the general southward flow of water from the Arctic basin into

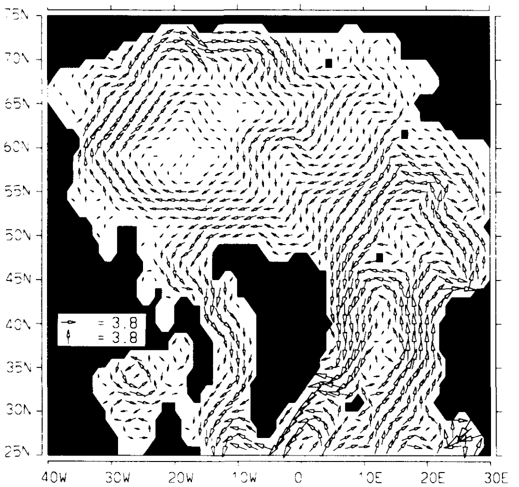

Fig. 5. Sea-surface velocity (cm/s) for 1 April.

the Archipelago (and ultimately into Baffin Bay) can be seen. Near the 20° W and 60° N (rotated coordinates) there is an anticyclonic gyre positioned over the Beaufort Sea. Furthermore, the gyre is not symmetric in shape, but is intensified towards the southwest (i.e., towards the Bering Strait). The dynamic height distribution of Coachman and Aagaard (1974) shows that it is in the southwestern Beaufort Sea (i.e., towards the direction of the Bering Strait) that the strongest gradient in the dynamic height occurs. From geostrophy, this is equivalent to saying that the largest velocities should occur in that part of the gyre, and indeed, the currents simulated in Fig. 5 reach maximum values in the southwestern part of the gyre. The maximum velocities in the gyre reach magnitudes of only 3 cm/s, which are in agreement with estimates from the dynamic height field as well as measurements taken with current meters during the AIDJEX experiment (Newton and Coachman, 1973).

To date, simulations of the surface circulation in the Arctic have shown that it exactly mimics that of the ice motion (e.g., see Fig. 11a of Hibler and Bryan, 1987). In using OPYC with a coarse resolution (i.e., a 2.0° spacing), similar results are obtained as in Hibler and Bryan (1987). That is, the surface circulation basically consists of one large anticyclonic gyre that spans the Arctic basin (Holland et al. 1995). However, even at the modest 1.0° resolution employed in this study, the mixed-layer velocity pattern (Fig. 5) deviates significantly from that of the sea-ice velocity (Fig. 4a). This single gyre concept for the surface circulation (which exactly mimics the flow of the sea-ice) is inconsistent with the observed dynamic height field, which suggests that there is a distinct anticyclonic gyre located only over the Beaufort Sea (i.e., not over the entire Canadian basin).

An important validation of the model's simulation of the surface currents is obtained by examining the surface currents in the vicinity of Fram Strait where the circulation is reasonably well observed. The bottom right-hand corner of Fig. 5 shows that the northward flowing Norwegian current splits into two branches as it meets the Barents Sea continental shelf break. One branch flows eastward into the Barents Sea, along the coast of the Barents Sea, then along the western coast of Novaya Zemlya, and finally into the Eurasian basin via the St. Anna Trough. The second branch of the Norwegian current flows towards Spitsbergen and joins up with the cyclonic Greenland Sea gyre. The surface flow through Fram Strait is southward and forms the East Greenland current, which itself appears to be intensified along the break of the east Greenland shelf. Consistent with the sea-surface velocity field is the sea-surface elevation field (Fig. 6). There is an elevation of about 60 cm over the Gulf Stream (not shown), and a sea-surface depression of about 55 cm in the GIN Sea. Over the Arctic basin, the sea-surface elevation implies the existence of an anticyclonic flow there. This is consistent with Fig. 5 because the sea-surface elevation reflects the pressure gradient which is forcing the mixed-layer flow. By contrast, dynamic heights do not absolutely specify the surface flow. Thus, the observed dynamic heights (Coachman and Aagaard, 1974) gives the flow at the surface relative to the flow at 1200 db. Since sea-surface elevation has never been accurately measured over the Arctic, one cannot use the dynamic heights to determine the surface circulation with absolute certainty. With this *caveat* in mind, we note that Fig. 6 gives a *relative* change of sea surface elevation of about 50 cm from the centre of the Beaufort gyre to Fram Strait. This relative change in sea-surface elevation is in agreement with the relative change in the observed dynamic heights between the same two locations (Coachman and Aagaard,

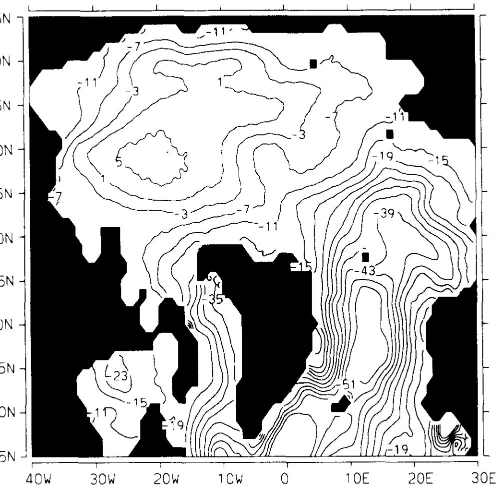

Fig. 6. Sea-surface elevation (cm) for 1 April. The highest elevation actually occurs over the Gulf Stream and is not shown in this limited domain figure. The lowest occurs in the Norwegian Sea (−55 cm) while over the Canadian basin there is a slight elevation (+5 cm) in the sea surface. Contour interval is 4 cm.

1974). Again, the accuracy of this comparison of relative changes in observed dynamic heights and modelled sea-surface elevation is valid only if there exists a level of no motion at 1200 db.

The mixed-layer depth distribution in the Arctic (Fig. 7) shows that the greatest depths occur in the GIN Sea and along the border between the Barents Sea and the Norwegian Sea. It was anticipated that the greatest values in the model should occur in the Greenland Sea since it is there that the greatest convective overturning takes place in reality. It is noted that the mixed-layer depth is extremely shallow everywhere else in the Arctic, except for a nominal deepening in the Laptev Sea and in the vicinity of the Bering Strait.

Associated with the mixed-layer depth distribution is the pattern of surface convection (Fig. 8). In the domain shown, the convection in the GIN Sea is the most intense (i.e., $\geqslant 130$ m). There is also substantial convection occurring in the Barents Sea (i.e., > 100 m). The convective waters formed on the shallow continental shelf of the Barents Sea may channel into the waters of the Eurasian basin via the St. Anna Trough and thus play a role in the formation of the subsurface waters (Coachman, 1962). It is also noted from Fig. 8 that convection occurs in the vicinity of the Bering Strait and in the Chukchi Sea, where sea ice is continually being formed and advected offshore. Consequently, this region may be an important contributor to the ventilation of the deeper waters in the Canadian basin. By contrast, convection does not occur over the Siberian shelves in this simulation as the water column is far too stable in that region. The convection in the vicinity of the North Pole is believed to

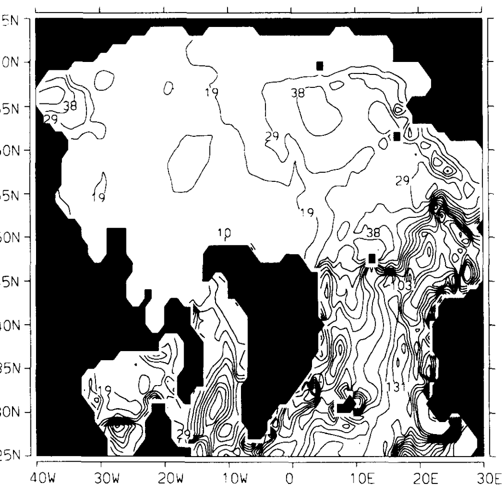

Fig. 7. Mixed-layer depths (m) for 1 April. The mixed-layer depth is greatest in the GIN Seas. In the Arctic, the greatest mixed-layer depths occur in the Barents Sea, the Laptev Sea, and the vicinity of the Bering Strait passage. Contour interval is 9 m.

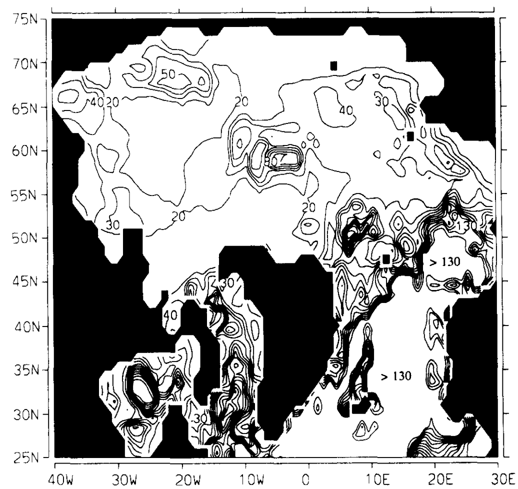

Fig. 8. Average depth of surface convection (m) for the month of March. The dominant area for convection in the Arctic basin is along the Barents Sea; however, some convection also occurs in the Beaufort, Chukchi and Laptev Seas. Contour interval is 10 m.

be an artifact of the surface salinity field used to force the model. The Levitus (1982) salinity data are generated on a Mercator grid and are in general not filtered to remove distortions that occur for values near the pole.

3.3. North–south transports

The exchange of ocean mass between the Arctic Ocean and the North Atlantic occurs in this model through three passages, namely, the Canadian Arctic Archipelago, Fram Strait, and the Barents Sea. We monitored the seasonal cycle of the exchange of ocean mass through these passages by taking transects across them throughout the seasonal cycle (Fig. 9a). The Arctic has a loss of about 0.7 Sv through the Canadian Arctic Archipelago, and a bigger loss of about 1.7 Sv through Fram Strait. At the same time the Arctic gains about 2.5 Sv through the Barents Sea. Thus there is rough balance of mass for this domain. There is some seasonal variation in the Barents Sea and Fram Strait flows, but not in the outflow of the Canadian Arctic Archipelago.

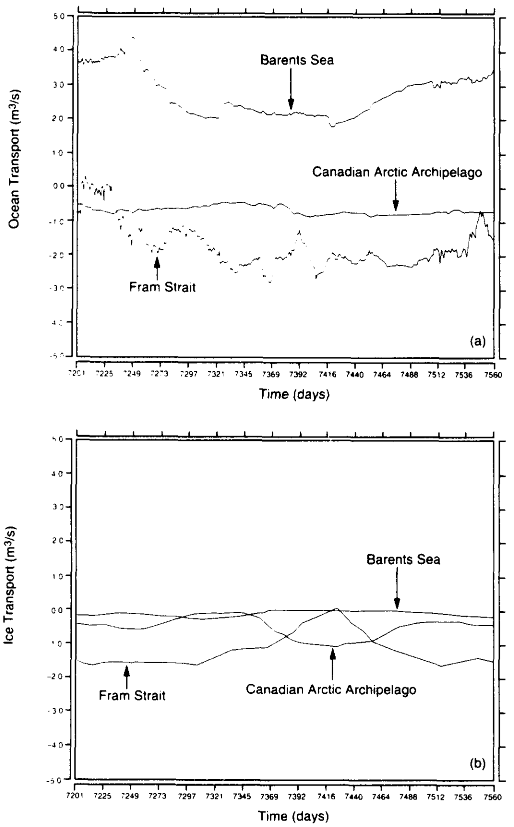

Fig. 9. (a) Ocean throughflows (Sv) in the Canadian Arctic Archipelago, the Fram Strait and the Barents Sea. (b) Ice throughflows (Sv) in the Canadian Arctic Archipelago, the Fram Strait and the Barents Sea.

Analogous to the exchange of ocean mass, the exchange of ice mass (Fig. 9b) was also monitored across the three passages that connect the Arctic with the rest of the model domain. The Canadian Arctic Archipelago shows an outflow with an average of 0.5 Sv, Fram Strait shows an outflow of average 1.1 Sv, and the Barents Sea shows an export of only 0.1 Sv. The seasonal cycle of outflow through the Canadian Arctic Archipelago is such that it peaks during summer, which is presumably because the ice has a greater freedom to flow during summer than in winter. By contrast, the outflow through Fram Strait is largest in winter.

3.4. Atlantic layer

Warm, saline Atlantic water penetrates into the Arctic Ocean via Fram Strait. This water is heavier than the surface Arctic waters and subducts as it travels north of Fram Strait, where it occupies the water column between 300 and 900 m below the surface. The simulation of the velocities, temperatures and salinities at the 500 m level are shown in Fig. 10. The velocity pattern at 500 m depth indicates that the waters at that depth are basically constrained to follow the bathymetry (see Fig. 1a). The modelled circulation in Fig. 10a consists of two cyclonic gyres which simply mimic the pattern of ocean subbasins (again, see Fig. 1a). The flow in the Eurasian basin consists of a large single-cell cyclonic gyre. Near the continental shelf break of the Laptev Sea, the Eurasian basin water is seen to flow on into the Canadian basin by flowing over the Lomonosov ridge. This circulation can be compared with the circulation inferred from temperature and salinity measurements which shows only a single basin-wide gyre. The modelled circulation pattern of a separate cyclonic gyre for each the Eurasian and Canadian basin is supported by observations taken during the Oden 91 North Pole Expedition (E. P. Jones, Bedford Institute of Oceanography, personal communication, 1992). During that expedition the concentration of various chemical tracers were measured at various locations over the Eurasian basin.

The modelled fields of temperature (Fig. 10b)

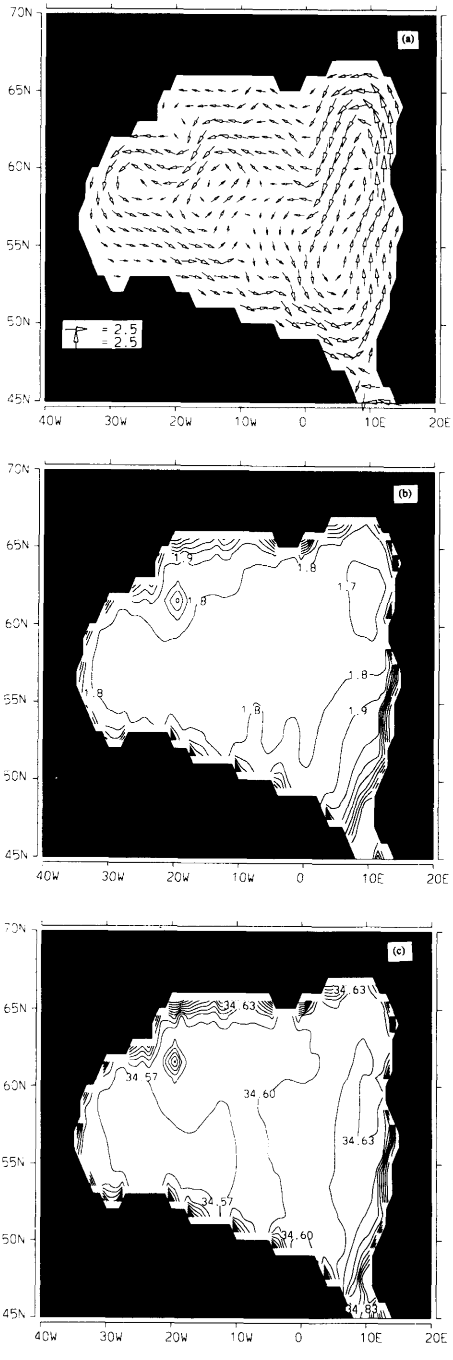

Fig. 10. (a) Velocity (cm/s) at 500 m depth on 1 April. (b) Temperature (°C) at 500 m depth on 1 April. Contour interval is 0.1°C. (c) Salinity (psu) at 500 m depth on 1 April. Contour interval is 0.030 psu.

and salinity (10c) show patterns that are consistent with the circulation pattern (Fig. 10a). The temperature field shows the warm, saline Atlantic water entering via Fram Strait. The temperature decreases as the water circulates cyclonically in the Eurasian basin. In this simulation, the warmest Atlantic layer waters are confined to the region of the continental shelf break of the Barents Sea (i.e., the Atlantic layer waters flow with the shelf break on their right hand side as they enter and circulate around the Eurasian basin). The simulated temperature is different from Semtner (1987, his Fig. 12) principally because although his Eurasian basin circulation had a cyclonic sense of flow as in the present study, his Canadian basin had a flow in the opposite sense to the cyclonic flow presented here. This difference in flow patterns explains the difference in the present study compared to that of Semtner (1987) in the simulation of the Atlantic layer waters as they are brought into the Arctic and circulated about.

A pool of relatively cold water is located in the centre of the Eurasian basin and another in the centre of the Canadian basin. The explanation for this pattern is believed to be due to the advection of the warm Atlantic water which occurs predominantly along the periphery of a basin. The temperature field (Fig. 10b) is credible in its spatial structure; however, the temperatures are too warm in the Canadian basin by about 1.0°C. Possible explanations for this excess heat have been discussed in Section 2.4.

The salinity pattern at 500 m depth shows the gradual freshening of the Atlantic layer water as it moves cyclonically from Fram Strait (34.83 psu) around the Eurasian basin and into the Canadian basin. In the centre of the Canadian basin there is a pool of relatively fresh water (34.57 psu). The nature of the equation of state for sea water is such that, at the low temperatures found throughout the Arctic basin, the density is completely controlled by the salinity. Consequently, Fig. 10c is in essence a horizontal slice of the isopycnals. Since the salinity shows low values in the centre of the Canada basin and the Eurasian basin, we can conclude that the isopycnal surfaces in each of these basins has a concave (facing upward) shape. This in turn implies a convex shape for the dynamic height at the surface of each of the basins, which is certainly in agreement with the observations, at least in the Beaufort Sea.

3.5. Deep layer

Below the top 500 m, the Arctic Ocean has little stratification. Consequently, the ocean response is expected to be basically barotropic in the deep ocean. The model simulations of velocity, temperature and salinity (Fig. 11) indicate patterns similar to that at 500 m (see Fig. 10). In the Eurasian basin the circulation has now become more complex, essentially because of the topographic impact of the Nansen-Gakel ridge (which subdivides the Eurasian basin into two subbasins). In the Canadian basin there is a single cyclonic flow consisting of a relatively fast and narrow equatorward flow and a broader and slower return flow towards the North Pole. There were measurements of the deep circulation in the Canadian basin taken by Hunkins et al. (1969). They used a photographic nephelometer to infer currents from light scattering. Their observations suggested a cyclonic deep circulation in the Canadian basin with speeds of 4 to 6 cm/s, with the currents primarily confined to the sloping margins of the basin. Furthermore, this pattern of deep circulation in the Canadian basin is in agreement with ideas and experiments on deep circulation with a concentrated source and distributed surface sink (Stommel et al., 1958).

The deep temperature (Fig. 11b) and salinity (Fig. 11c) fields show similar horizontal structure, in that they have patterns which mimic the bathymetry beneath them, in both the Canadian and Eurasian basins. The horizontal variations in temperature and salinity at a depth of 2500 m are such that there is relatively warm, fresh water in the centre of these basins relative to the colder, saltier water found around the periphery of the basins.

Of concern, with regards to the temperature and salinity patterns of Figs. 11b, c, is that the patterns are more or less terrain-following. This may be partly due to the interpolations scheme in going from the model's Lagrangian coordinates to the Eulerian coordinates of Figs. 11b, c. Also of concern is that the model's vertical resolution (see Fig. 1b) is poor for the deep waters. This will be improved in future work by using a higher resolution.

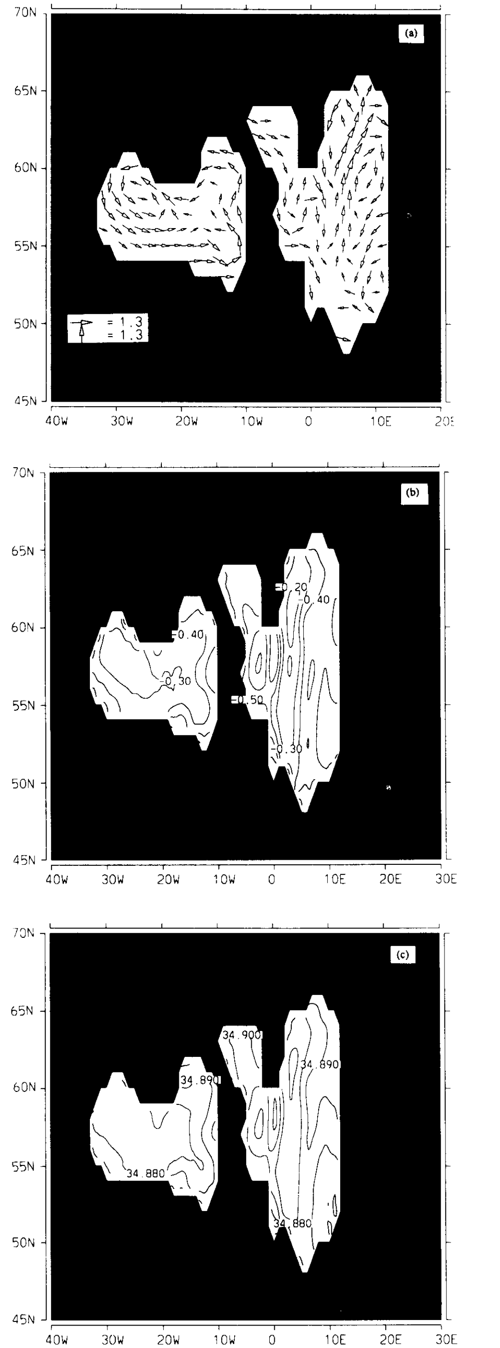

Fig. 11. (a) Velocity (cm/s) at 2500 m depth on 1 April. (b) Temperature (°C) at 2500 m depth on 1 April. Contour interval is 0.10°C. (c) Salinity (psu) field at 2500 m depth on 1 April. Contour interval is 0.010 psu.

3.6. Two-dimensional transects

An alternate view of the simulated fields of temperature and salinity is offered by taking two-

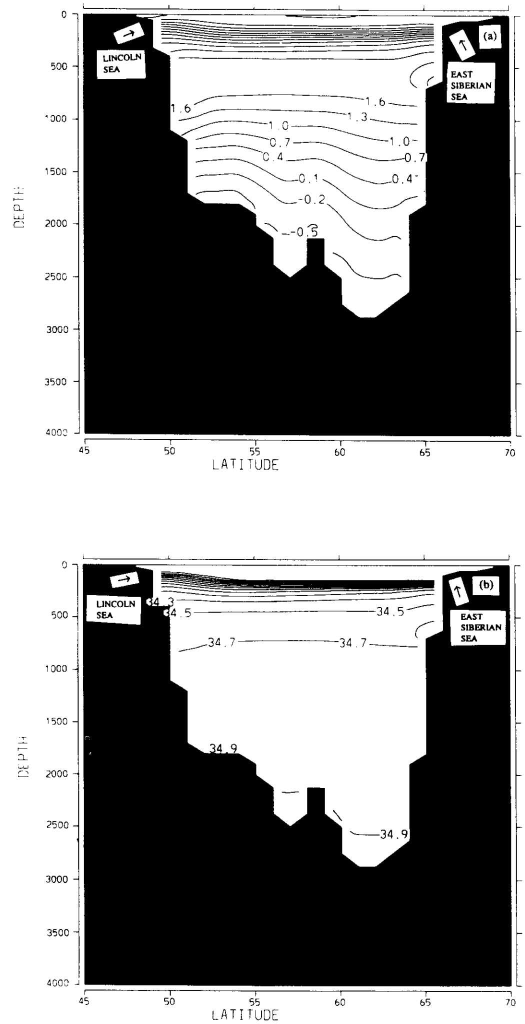

Fig. 12. (a) North–south transect (rotated coordinates) showing the distributions of temperature (°C) on 1 April. The black area represents ocean bottom topography. The transect is taken at a rotated longitude of 7° W (refer to Fig. 1a for orientation). Contour interval is 0.30°C. (b) As in figure (a) but showing the distributions of salinity (psu) on 1 April. Contour interval is 0.200 psu.

dimensional transects of the model output. All the geographical headings referenced below refer to that of the model domain coordinates (which are rotated with respect to geographical coordinates). The rotated model domain coordinates are labelled along the axes of all plots. First, from a vertical slice in a rotated north–south direction positioned at 7° W (see Fig. 1a for orientation), one can see how the warm, saline Atlantic layer water has positioned itself at an average depth of about 500 m, and that it is warmest near 65° N, which is consistent with the advection of the Atlantic layer water from the Eurasian basin into the Canadian basin along the Siberian shelf. Secondly, from a vertical slice in a rotated east–west direc-

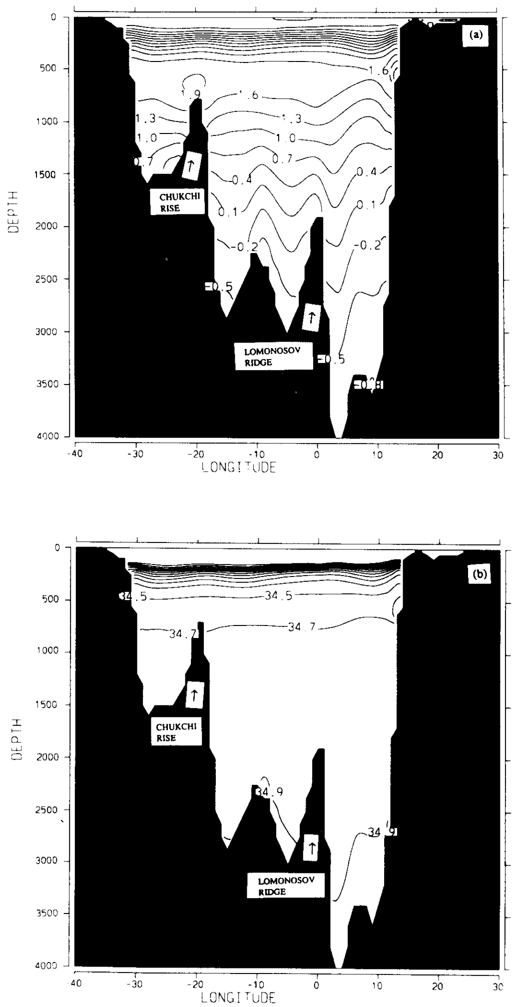

Fig. 13. (a) East–west transect (rotated coordinates) showing the distribution of temperature (°C) on 1 April. The black area represents ocean bottom topography. The transect is taken at a rotated latitude of 61° N (refer to Fig. 1a for orientation). Contour interval is 0.30°C. (b) As in figure (a) but showing the distribution of salinity (psu) on 1 April. Contour interval is 0.200 psu.

tion positioned at 61° N (again, see Fig. 1a for orientation), one can see that the warmest and saltiest of the Atlantic layer water has spread all the way into the Canadian basin (see Fig. 13).

3.7. Barotropic stream function

The barotropic stream function represents the vertically averaged flow. This stream function indicates anticyclonic flow for the subtropical gyre (not shown) and cyclonic flow (up to 15 Sv) for the GIN Sea (Fig. 14). For the Arctic basin, the depth averaged transport is cyclonic for both the Canadian and Eurasian basins (Fig. 14), it being more intense for the Eurasian basin (10 Sv) than for the Canadian basin (6 Sv). In this model simulation, the generally anticyclonic transport of the surface waters in the Canadian basin is dominated by the cyclonic deeper transports producing an overall net cyclonic transport in that basin. This is exactly opposite to the results of Hibler and Bryan (1987) and Semtner (1987).

In the past many have believed that the depth-averaged flow over the Canadian basin is generally of an anticyclonic sense, consistent with it being forced by the wind (via the ice). Indeed, the wind stress curl into the Canadian basin is anticyclonic (as evident from Fig. 3). The surface waters of the Canadian basin, as simulated in this study (Fig. 5), also have an anticyclonic flow; however, the

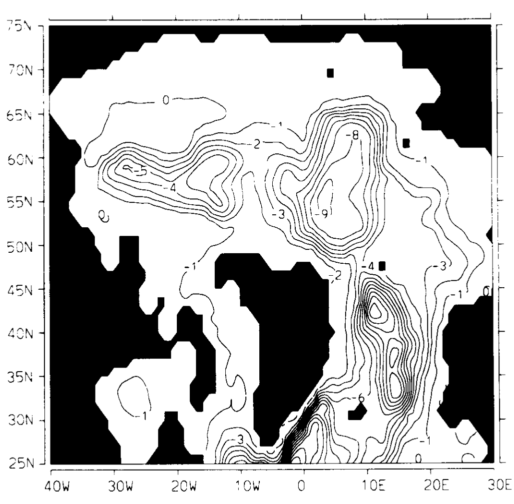

Fig. 14. Barotropic stream function (Sv) on 1 January. Contour interval is 1 Sv.

deeper waters have a cyclonic sense (Fig. 11a). In this model, the deeper cyclonic waters have a greater net transport than the upper anticyclonic waters. As the pycnocline occurs at a relatively shallow depth of about 300 m over the Canadian basin, it is possible that the slower, deeper cyclonic flow dominates the net transport simply because it has a much greater depth over which it flows compared to the faster moving but relatively thinner water column above the pycnocline.

It is possible that the Canadian basin has a net cyclonic flow despite the fact that the surface forcing imparts an anticylonic torque on the water column. This apparent inconsistency between the sense of the surface forcing field (the wind being anticyclonic) and that of the total response field (the vertically-averaged ocean going cyclonic) may be resolved if one considers the role of the haline driven circulation. Generally, the water of the GIN Sea is more saline than that of the Arctic. This denser GIN Sea water thus flows into the Arctic and flushes the Arctic water back out into the GIN Sea. Under geostrophic balance, it would be plausible for the GIN sea water to flow into the Arctic in such a manner that it flows in a cyclonic sense, that is with the continental shelves on its right. This conceptual picture of the Eurasian and Canadian basin flows being driven by the denser water of the GIN Sea is at least consistent with the Eurasian basin having a stronger flow (−10 Sv, Fig. 14) than that of the Canadian basin (−6 Sv, Fig. 14). If the basic forcing for the flow in the Arctic comes from the density contrast between the various basins, then certainly the Eurasian basin is subject to a greater forcing than that of the Canadian basin. The above mechanism is speculative, but its outline does serve to highlight a profitable area for future research. A rigorous answer will require a diagnostic analysis of the various torques on the water column and that is beyond the scope of this preliminary investigation.

The picture suggested is that the Arctic is a haline driven ocean and that the wind forcing is only of secondary importance. To better understand what drives the flow, a complete diagnostic budget was performed on all the terms of eq. (6) for the momentum balance. Of all the terms in eq. (6), the pressure gradient term is the dominant one. Of course, the Coriolis term is roughly equal in magnitude (and opposite in sign) to the pressure term, but it is just a response to forcing and does not force motion of its own accord. Referring back to Fig. 1b, which shows an example of the model's vertical coordinate system at a particular instant in time, one can see the location of the mixed layer (1st layer) and the bottom layer (11th layer). The pressure gradient term for the mixed layer (Fig. 15a) and the bottom layer (Fig. 15b) shows that the pressure gradient points everywhere towards the centre of the GIN Sea in both the mixed layer and the bottom layer. By contrast the pressure gradient over the Canadian basin switches its sense when going from the mixed layer to the bottom layer.The pressure gradient patterns (which drive the motion) are then consistent with the GIN Sea not having a strong pycnocline and not being able to reverse its flow sense with depth (i.e., no baroclinicity) whereas the Canadian basin has a strong pycnocline and has the ability to change its flow pattern with depth (i.e., baroclinicity). The pressure gradient fields of Fig. 15 exist in this model because of the salinity. In a sensitivity experiment (Holland et al., 1995) in which the wind-driven component of the flow was eliminated (by turning off the wind stress), the barotropic stream function (Fig. 14) was not greatly affected in the Arctic. To reiterate, the pressure gradient field of the deeper waters (Fig. 15b) arises from the salinity contrasts between the various basins and this is of first-order importance to the general circulation of the Arctic. Further studies are required to elucidate the processes and mechanisms that determine the set up of the pressure field throughout the Arctic Ocean.

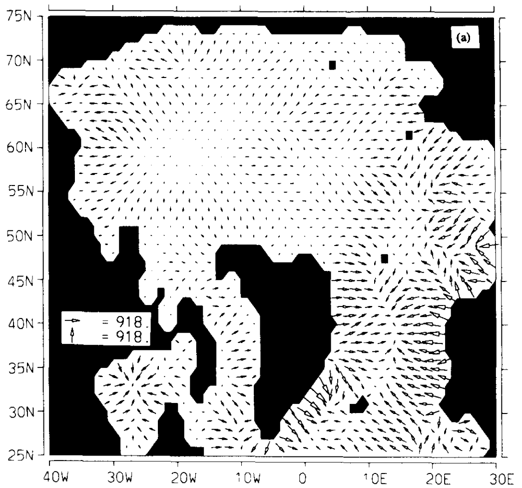

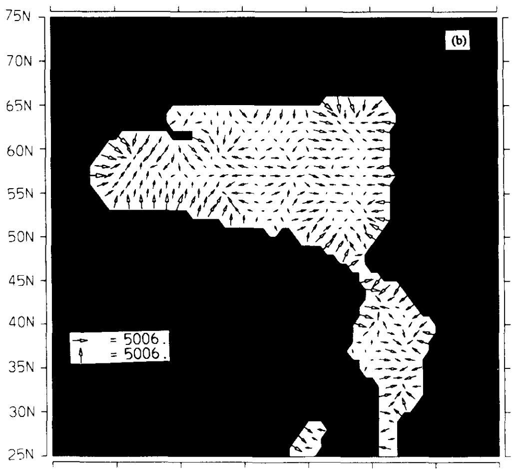

Fig. 15. (a) Diagnosed pressure gradient term of the momentum equation for the mixed-layer (1st layer) of the isopycnal model. (b) As in (a) but for the bottom-layer (11th layer) of the isopycnal model.

4. Conclusions

The key results of the study are now highlighted. The sea-ice thickness simulation (Fig. 4) is satisfactory in that it did reproduce the climatologically distribution of both thickness and velocity field.

The mixed-layer circulation indicated the presence of an anticyclonic gyre (Fig. 5) centred over the Beaufort Sea in the Canadian basin. The mixed-layer depths (Fig. 7) were relatively shallow in the Arctic, and deep over the Barents Sea. They were also relatively deep in the Laptev Sea and in the vicinity of the Bering Strait. The model indicated convection (Fig. 8) of surface waters to great depths over the Barents Sea, and again to a lesser but substantial depths over the Laptev Sea, the Chukchi Sea, and in the vicinity of the Bering Strait. Indeed these regions three regions may be of key importance in ventilating the Atlantic layer and deeper waters of the Arctic Ocean; however, based on the excessively warm Atlantic layer temperatures simulated, it would seem that insufficient convection occurred in the present simulation.

The horizontal exchange of the Arctic waters with the North Atlantic via the Canadian Arctic

Archipelago, Fram Strait, and the Barents Sea indicated that on an annual average, there was a rough balance of the outflow through the Canadian Arctic Archipelago and Fram Strait with that of the inflow through the Barents Sea. By contrast, the model simulated a net flow of ice out of the Arctic basin.

The penetration and subduction of warm, salty water into the Arctic Ocean from the North Atlantic via Fram Strait is clearly evident throughout the Arctic (Figs. 12 and 13). This water forms the Atlantic layer and is the dominant feature at a depth of 500 m. The flow is everywhere cyclonic (Fig. 10a) in the basin and thus is, in many places, reversed in its sense of direction as compared to the surface circulation. Thus, for example, the Beaufort Sea has a surface anticyclonic gyre overlying a deeper cyclonic flow, which implies strong vertical shears below the mixed layer. The simulated water temperatures were in general too high by about 1.0°C (Fig. 10b). This excessive heat may be the result of a poor parameterization of convection, or alternatively of poor vertical resolution (see Fig. 1b). The simulated salinities indicated lower values in the centre of the cyclonic gyres. This is consistent with the requirement that the isopycnals slope in a manner to give flow reversal of the Atlantic layer waters with respect to the mixed layer.

The deeper flow at 2500 m is also everywhere cyclonic. The most notable feature of the deeper flow is that it more closely followed along bathymetric contours (Fig. 11a) than the Atlantic layer flow. It was also seen that the deeper flow was intensified along certain boundaries. The simulation of the temperature (Fig. 11b) and salinity (Fig. 11c) at these depths produced patterns that mimicked the bathymetric patterns.

One must exercise caution in the interpretation of the simulation results presented here because of the artificial boundaries and the relatively short integration time. A further limitation was the use of only 11 discrete isopycnal layers in the vertical and 1.0° spacing in the horizontal. This choice was dictated by the limited computing resources available. Future studies will involve an increased number of vertical layers, increased horizontal resolution, and an increased model domain to include part of the northern Pacific so as to include the exchange through Bering Strait. As an alternative to an increased model domain, open boundary conditions may be employed. This model will be used to study the interannual and interdecadal variability of the Arctic with respect to wind forcing and river runoff (Mysak and Power, 1992, for a motivation of this work).

The application of the OPYC coupled sea ice, mixed layer, isopycnal ocean general circulation model to the Arctic Ocean has proved useful in simulating many of the known circulation and water-mass properties. The OPYC model is presently used in global climate studies (coupled to an atmospheric model, see Lunkeit, 1993), and it is the purpose of studies such as the present one to describe in detail the performance of the Oberhuber model in a particular region (the Arctic Ocean). The numerous parameters used in this study were chosen to be the same as those used in global domain studies. This was done for two reasons. First, it does not seem reasonable to tune the model parameters to obtain an optimal simulation for the Arctic Ocean, while at the same time knowing that a different set of parameter values are used when the model is run in a global domain. Secondly, the present generation of supercomputers are still inadequate in terms of computational speed to be able to perform a sensitivity study of the model to its large number of parameters and parameterizations.

5. Acknowledgments

We are grateful to Cray Research Inc. for providing computing time on a Cray located at the National Centre for Atmospheric Research (NCAR). It is with equal gratitude that we acknowledge the computing time provided by The Arctic Region Supercomputing Center (ARSC) on their Cray located at the University of Alaska. The assistance of Mr. Chuck Swanson of Cray Research Inc. in particular is very much appreciated as is that of Ms. Dorothy Corbett of ARSC. D. M. Holland thanks the Newfoundland Government Career Development Awards Programme and the Canadian Atmospheric Environment Service (AES) for graduate support. L. A. Mysak is grateful for research support from the AES and the Canadian Natural Sciences and Engineering Research Council. J. M. Oberhuber is grateful for support from the German Bundesminister für Forschung und Technologie.

REFERENCES

Aagaard, K. 1989. A synthesis of the Arctic Ocean Circulation, *Rapp. P. V. Reun. Cons. Int. Explor. Mer.* **188**, 11–22.

Aagaard, K. and Carmack, E. C. 1989. The role of sea ice and other fresh water in the Arctic circulation. *J. Geophys. Res.* **94**, 14485–14498.

Aukrust, T. and Oberhuber, J. M. 1995. Modelling of the Greenland, Iceland, and Norwegian Seas with a coupled sea ice, mixed layer, isopycnal ocean model. *J. Geophys. Res.*, in press.

Bourke, R. H. and Garrett, R. P. 1987. Sea ice thickness distribution in the Arctic Ocean. *Cold Regions Science and Technologie* **13**, 2107–2117.

Carmack, E. C. 1990. Large-scale physical oceanography of polar oceans. In: *Polar oceanography, Part A, Physical science*, (ed. Smith). Academic Press, New York, 171–222.

Coachman, L. K. and Barnes, C. A. 1962. Surface water in the Eurasian Basin of the Arctic Ocean. *Arctic* **15**, 251–277.

Coachman, L. K. and Aagaard, K. 1974. Physical Oceanography of Arctic and Subarctic Seas. In: *Marine geology and oceanography of the Arctic seas* (ed. Herman), Springer-Verlag, New York, 1–72.

Colony, R. L., Rigor, I. and Runciman-Moore, K. 1991. A summary of observed ice motion and analyzed atmospheric pressure in the Arctic Basin, 1979–1990. Tech. mem. APL-UW TM13-91, University of Washington, Seattle, Wash., 106 pp.

Cox, M. D. 1984. *A primitive equation, three-dimensional model of the ocean*. GFDL Ocean Group Tech. Rep. No. 1, GFDL/NOAA, Princeton University, Princeton, 250 pp.

Galt, J. A. 1973. A numerical investigation of Arctic Ocean dynamics. *J. Phys. Oceanogr.* **3**, 379–396.

Garwood, R. W. Jr., Gallacher, P. C. and Müller, P. 1985. Wind direction and equilibrium mixed-layer depth. General Theory. *J. Phys. Oceanogr.* **15**, 1525–1531.

Heirtzler, J. R. (ed.) 1985. *Relief of the surface of the earth*. Rep. MGG-2, National Oceanographic and Atmospheric Administration, Boulder.

Hibler, W. D. III, 1979. A dynamic thermodynamic sea-ice model. *J. Phys. Oceanogr.* **9**, 815–846.

Hibler, W. D. III and Bryan, K. 1987. A diagnostic ice-ocean model. *J. Phys. Oceanogr.* **17**, 987–1015.

Holland, D. M. 1993. *Numerical simulation of the Arctic sea ice and ocean circulation*. PhD thesis, McGill University, Montreal, Quebec, 203 pp (available as McGill Centre for Climate and Global Change Research Rep. 93-4).

Holland, D. M., Mysak, L. A., Manak, D. K. and Oberhuber, J. M. 1993. Sensitivity study of a dynamic-thermodynamic sea-ice model. *J. Geophys. Res.* **98**, 2561–2586.

Holland, D. M., Mysak, L. A. and Oberhuber, J. M. 1995. Simulation of the mixed-layer circulation of the Arctic Ocean. *J. Geophys. Res.*, in press.

Hunkins, K., Thorndike, E. M. and Mathieu, G. 1969. Nepheloid layers and bottom currents in the Arctic Ocean. *J. Geophys. Res.* **74**, 6995–7008.

Legates, D. R. and Willmott, C. J. 1990. Mean seasonal and spatial variability in gauge-corrected global precipitation. *Internat. J. Climatol. Res.* **9**, 111–127.

Levitus, S. 1982. *Climatological atlas of the world ocean*. NOAA Publ. 13, US Dept. of Commerce, Washington, DC, 173 pp.

Lunkeit, F. 1993. *Simulation der interannualen variabilitat mit einem globalen gekoppelten atmosphare-ozean modell. Berichte aus dem Zentrum fur Meeres und Klimaforschung*, Reihe A, Nummer **8**, PhD Thesis.

Mysak, L. A. and Power, S. B. 1992. Sea-ice anomalies in the western Arctic and Greenland–Iceland Sea and their relation to an interdecadal climate cycle. *Clim. Bull.* **26**, 147–176.

Newton, J. L. and Coachman, L. K. 1973. 1972 AIDJEX interior flow field study preliminary report and comparison with previous results. *AIDJEX Bulletin* **19**, 19–42.

Niiler, P. P. and Krauss, E. B. 1977. One-dimensional model of the seasonal thermocline. *The Sea* **VI**, Wiley Interscience, 97–115.

Oberhuber, J. M. 1988. *An atlas based on the COADS data set. The budgets of heat, buoyancy, and turbulent kinetic energy at the surface of the global ocean*. Max-Planck-Institute for Meteorology, Hamburg, Report 15, 199 pp.

Oberhuber, J. M. 1993a. Simulation of the Atlantic circulation with a coupled sea ice, mixed layer, isopycnal general circulation model. Part I: Model Description. *J. Phys. Oceanogr.* **23**, 808–829.

Oberhuber, J. M. 1993b. Simulation of the Atlantic circulation with a coupled sea ice, mixed layer, isopycnal general circulation model. Part II: Model Experiment. *J. Phys. Oceanogr.* **23**, 830–845.

Oberhuber, J. M., Holland, D. M. and Mysak, L. A. 1993. A thermodynamic-dynamic snow sea-ice model. *Ice in the climate system*. NATO ASI Series, Series I: Global Environmental Change, W. R. Peltier (ed.), 653–673.

Ranelli, P. H. and Hibler, W. D. III, 1991. Seasonal Arctic sea-ice simulations with a prognostic ice-ocean model. *Annals of Glaciology* **15**, 45–53.

Ries, J. E. and Hibler, W. D. III, 1991. Interannual characteristics of an 80 km resolution diagnostic Arctic ice-ocean model. *Annals of Glaciology* **15**, 155–162.

Rudels, B., Jones, E. P. and Anderson, L. G. 1993. Atlantic water in the Arctic Ocean. Abstracts of the 27th Canadian Meteorological and Oceanographic Society Congress, Fredericton, New Brunswick, 93.

Semtner, A. J. Jr. 1976. Numerical simulation of the

Arctic Ocean circulation. *J. Phys. Oceanogr.* **6**, 409–425.

Semtner, A. J. Jr. 1987. A numerical study of sea ice and ocean circulation in the Arctic. *J. Phys. Oceanogr.* **17**, 1077–1099.

Stommel, H., Arons, A. B. and Faller, A. J. 1958. Some examples of stationary planetary flow patterns in bounded basins. *Tellus* **10**, 179–187.

Trenberth, K. E., Olson, J. G. and large, W. G. 1989. A global ocean wind stress climatology based on ECMWF analyses. NCAR Technical Note. *NCAR/TN-338-STR*, Boulder, Colorado.

Warn-Varnas, A., Allard, R. and Piacsek, S. 1991. Synoptic and seasonal variations of the ice-ocean circulation in the Arctic: A numerical study. *Annals of Glaciology* **15**, 54–62.

Wright, P. 1988. *An atlas based on the COADS data set: fields of mean wind, cloudiness, and humidity at the surface of the global ocean.* Max-Planck-Institute for Meteorology, Hamburg, Report 14, 70 pp.